Cronfa - Swansea University Open Access Repository

_____

This is an author produced version of a paper published in:
Wind Energy

_____

Cronfa URL for this paper:

_____

Paper:

Experimental and CFD Analysis of Stall Cells on Rectangular Wings

Marinos Manolesos[1], Georgios Papadakis[1], Spyros G. Voutsinas[1]

[1]Laboratory of Aerodynamics, National Technical University of Athens, 9 Heroon Polytechneiou str., 15780 Athens, Greece. E-mail: marinos@fluid.mech.ntua.gr. Tel: +30 6932 401959, Fax: +30 210 7721057

Abstract

The present article is the second part of a combined (experimental and computational) study on stall cells (SCs) on a rectangular wing. In the first part tuft data were used in order to geometrically characterise a stabilized SC resulting from a localised spanwise disturbance introduced by a zigzag (ZZ) tape. Here, pressure measurements on the model and in the wake, and aerodynamic polars at mid span are reported. The wing model had an aspect ratio (AR) value of 2, the Reynolds number was 10^6 and the range of angles of attack (α) was from -6º to 16º. Experimental results confirm previous findings. Furthermore, 2D and 3D RANS simulations are used in order to better understand the structure of SCs. 3D simulations reproduce the experimental data with a 3^0 delay in α and permit a qualitative analysis. It is found that the SC vortices start normal to the wing surface and extend downstream in the wake; the evolution of the SC vortices in the wake is in strong interaction with the Separation Line Vortex and the Trailing Edge Line Vortex; as the SC vortex develops downstream in the wake, its centreline is contracted towards the SC centre; the wing wake is pushed upstream at the centre of the SC and downstream at the sides by the SC vortices; spanwise lift and drag distributions always attain their minimum at the SC centre.

Keywords

Stall Cells, 3D CFD, Wing Aerodynamics, Experimental Aerodynamics

Introduction

Stall cells (SCs) are large scale three-dimensional (3-D) coherent structures that consist of two counter rotating vortices. Among other cases (e.g. see [1]), they are also formed on the suction side of airfoils that experience trailing edge (TE) stall including airfoils designed for or used on wind turbine blades ([2]–[4]). Although SC formation has been studied for a long time [5], the current state of knowledge around them remains limited. A survey on previous work can be found in [4].

1

The relevance of SCs to wind energy is twofold. Firstly, they have been observed on wind tunnel airfoil models that are used in order to create aerodynamic polars, which in turn are used in the design of wind turbines. Secondly, computational results [6] suggest that they are formed on wind turbine blades at standstill, an operation condition of particular interest in designing wind turbine blades because of its connection to flutter. In both aspects a deeper understanding of the phenomenon is necessary in order to correctly predict the loads on blades.

To date no reference of a SC on a rotating wind turbine blade has been made and it is still unknown how a SC would behave under radial pressure gradients. However, before dealing with the rotating case the stationary one should be better understood.

There is general agreement that SCs are dynamic structures that can be unstable, i.e. they can change in number and size or even move in the spanwise direction of a wing without any change in conditions, e.g. [5], [7]–[9]. In [4] it has been shown that a localized spanwise disturbance stabilizes the flow in a single SC at the centre of a rectangular wing. The resulting SC had the same amount of separated flow on the wing surface, but was first formed 2 degrees earlier than in the undisturbed cases. In [4] a geometrical characterization of the SCs was performed, whereas in the current paper pressure and CFD data are presented.

While some extensive experimental studies have been published in the past on SCs e.g. [1, 6, 9], this is not the case for CFD simulations. To the authors' best knowledge the only existing computational analysis is that of Zarutskaya and Arieli [9], who used RANS simulations and examined SCs on a NACA 0012 and a supercritical NASA SC2 airfoil at Reynolds (Re) number of $0.39 \ 10^6$ and $4.6 \ 10^6$.

Zarutskaya and Arieli [9] presented surface oil flow lines and wake contours along with a general schematic presentation of the SCs. However, the complex vortex structures involved in this case were not discussed. Relevant is also the work of Rodríguez and Theofilis [11] who, based on global stability analysis, attribute the onset of SCs to spanwise instabilities, albeit at a very low Re number of 200.

The present paper reports on the findings of the experimental and computational analysis of a plane rectangular wing that experiences 3-D separation with SCs at free stream Re number of 1.0×10^6 (Mach = 0.075). First the experimental and computational approaches are explained. Then the results are presented and discussed before summarizing the findings in the final section.

Experimental Setup and Procedure

Wind tunnel

All experiments were carried out in the 1.4mx1.8m test section of the National Technical University of Athens wind tunnel. The wind tunnel is of the closed single-return type with a total circuit length of 68.81 m. The circuit has a contraction ratio of 6.45:1. The free-stream turbulence level in the 3.75 m long octagonal test section is 0.2%.

Model

The tests concerned an 18% thick airfoil optimized for use on variable pitch and variable speed multi MW blades [12]. It belongs to the flat-top type experiencing TE separation leading to a gradual built-up of the lift and smooth post stall behaviour.

The wing model had a chord of 0.6m and spanned the test section vertically in order to minimize blockage. The solid blockage of the model reached a maximum of 9.2% at the highest angle of attack (α), 16°, i.e. below the 10% limit, see [13]. Furthermore, in order to minimize the effect of the wind tunnel boundary layer, side fences were used (Fig. 1, left). On the right half of Fig. 1 a schematic side view of the test set up is given.

Stabilization of the SCs

Zigzag (ZZ) tape was applied on the wing suction surface, centrally, for 10% of its span. This was done in order to apply a large enough spanwise disturbance to the flow that would stabilize the three-dimensional separation occurring at large enough angle of attack. For more details see [4]. All data in the current report refer to the case with the ZZ tape on, unless otherwise stated.
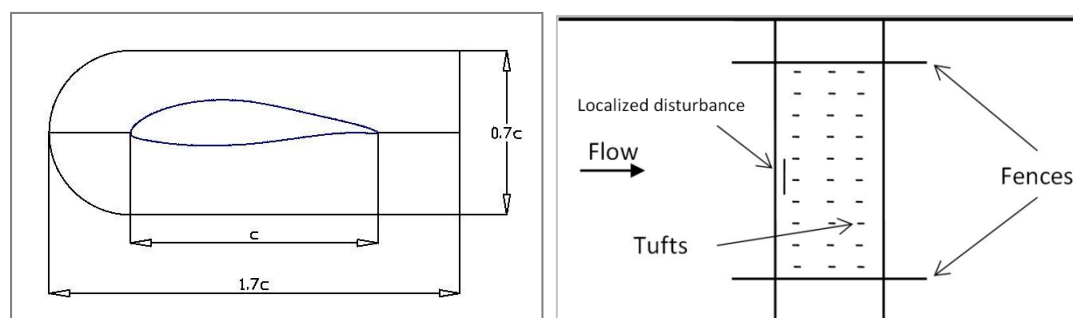

Fig. 1: (left) The fences shape and dimensions (1.7c long, 0.7c wide), (right) Side view of the test set up

Instrumentation

The model had 62 pressure taps located at the centre of the wing span. They extended from the leading edge to 88.8% of the chord in the chordwise direction. The wake rake was 39.1cm wide and consisted of 45 total pressure tubes and two static pressure tubes, located on a plane parallel, but offset compared to the rake

plane. All tubes were connected to a Scanivalve sensor and then through a 16 bit A/D card to the lab computer.

The wake rake was positioned on the traverse table 0.8c behind the wing TE and could move both in the spanwise direction and normal to the wing span. When the wake was wider than the rake width a second measurement would be taken after the rake was moved normal to the wing span with sufficient overlapping. The rake spanwise travel region was 84cm and covered +/-35% span. Positive/negative span values refer to locations above/below the wing mid-span, respectively, so that the full span of the wing extends from -50% (lowest point) to +50% (highest point).

Procedure

For this set of experiments the wing aspect ratio (AR) was set to 2.0 and the Re number was $1.0x10^6$. For each set of measurements first the targeted free stream velocity was reached and then the model would be set at the desired angle of attack. The wing pressure measurements were then followed by the wake pressure measurements. The wake was measured at different span positions from -35% to +35% in steps of 5% span (6cm). All measurements were taken at 200Hz for 5 seconds. A constant misalignment of the model with the flow by 0.2^o is allowed for in the results.

Force Coefficients

The lift coefficient (Cl) was computed from the pressure distribution around the airfoil. Since the pressure taps only covered up to 88.8% of the chord, the values reported in the present study are not the full Cl of the profile. When CFD data are compared with experimental data, then the computational lift coefficient is also computed by integrating up to 88.8%c for a fair comparison.

For attached flow conditions the drag coefficient (Cd) was computed from the wake pressure distribution according to [13]. For separated flow (α>6° in this case, or after a SC is initially formed) the pressure drag was used instead.

As expected, Cd varied considerably over the wing span, especially at higher angles of attack, due to the three-dimensionality of the wake. This meant that the Cl obtained from the wing pressure taps only corresponded to the flow conditions at the centre of the wing and not to the complete wing. The same holds for the drag coefficient computed at the centre of the wing. As a convention, however, the force coefficients at the centre of the wing will be referred to as the *wing Cl and Cd*, even though this is not literally true.

In order to estimate the pressure drag an approximation had to be used for the part of the chord that had no pressure taps (x>88.8%c). It was assumed that the pressure on the suction side remained constant through the separated flow region up to the

trailing edge. Then a second order approximation for the pressure on the pressure side was used. No such approximation was used for the Cl computation.

Wind tunnel corrections

Wind tunnel corrections were applied to the measured data according to [13], namely corrections for the case of a wing spanning the tunnel height. However, these corrections have been developed with the assumption of a two-dimensional flow. Even though the effect of the corrections is small, it has to be mentioned that their application in the present study is somewhat problematic since, as it will be shown, when a SC is formed the wake becomes highly three-dimensional.

Tuft data

In this report some tuft visualisation data from [4] are also presented for reference and validation purposes. In particular the following metrics were used:

a) The SC width as % of the span (SC width = z/S)
b) The most upstream x/c location of the SC boundary (earliest separation point)

These are defined in Fig. 2, where a snapshot from the tuft visualisation experiments is shown (case: AR 2.0, Re $1.0x10^6$, 9.0° with ZZ tape). A tuft would be considered "belonging to a SC" if it would deviate from the chordwise direction most of the time during a run. More photos and videos are available in [4], [14]
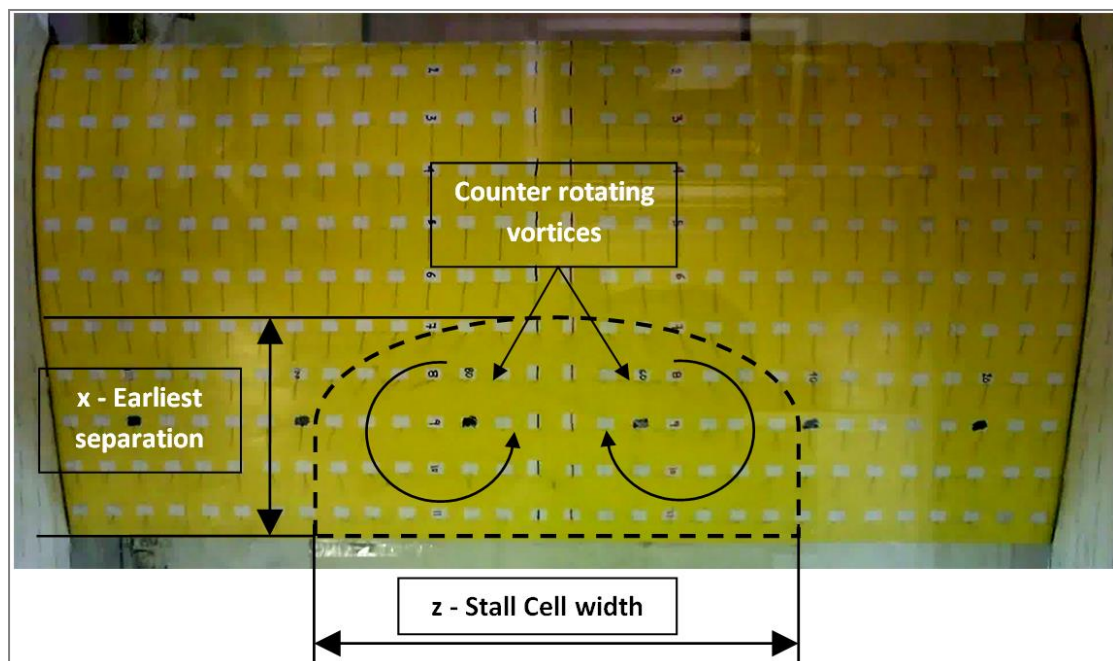

Fig. 2: Schematic view of a SC for AR=2.0, Re=1.0x10⁶, a=8.0°, locally tripped at the wing span centre. The direction of the flow is from top to bottom.

Computational approach

Solver

The (U)RANS solver used in the present work is a MPI parallelised, multi-block finite volume compressible code applied to mixed structured/unstructured grids. The code is equipped with pre-conditioning for low Mach flow conditions and uses the Spalart-Allmaras turbulence model. The discretisation is 2nd order accurate in time and space while dual time stepping is introduced in order to facilitate convergence.

An important issue is that of turbulence modelling. In Zarutskaya and Arieli [9], in addition to the Spalart - Allmaras (S-A) one equation model [15], also Menter's k-ω SST model [16] was used. They found that the S-A model predicts stall with delay, i.e. at a greater angle of attack than expected. Regarding turbulence modelling it is accepted [17] that eddy viscosity models in general are not sufficient for modelling three-dimensional turbulent vortical flows as they erroneously produce eddy viscosity in the vicinity of free vortices, which causes the vortices to be excessively diffused above and beyond the effects of insufficient grid resolution. In this sense, the choice amongst various eddy viscosity models is not regarded essential in view of the qualitative analysis targeted in this work.

Grid

A c-type grid was used that extended 50 chords around the airfoil. The boundary layer mesh ensured the y+ value was lower than 1 throughout the wing surface. In order to create the 3D grid, the 2D grid (which was used for the two-dimensional calculations) was extruded in steps ranging from 0.0248 at the centre of the span to 0.0646 non-dimensional length units at the tip. The grid covered half of the span. At one end symmetry condition was used while at the other (fence position), inviscid wall boundary conditions were implemented. SCs are not a tip effect [18] and fully resolving the complex corner flow between the wing and the fence was not the aim of this study. The result was a computational domain, which will be referred to as the baseline grid. The symmetry condition had no effect on the results.

Table 1 below summarizes the details and some of the results for the grid cases tested. The differences in results between the baseline grid (0.9×10^6 cells) and the denser grids were at the order of 1% for Cl and 7% for Cd at $\alpha = 9^o$. Still, it was decided to proceed with the baseline grid due to the computational cost. It was not possible to run higher density meshes with the available resources.

Zigzag tape modelling

The flow in the experiments was locally disturbed for 10% of the wing span on the suction side using a 0.4mm thick ZZ tape of 60°. According to Elsinga and Westerweel [19] undulating spanwise vortices are shed from zigzag tape edge, which lead to turbulence. In the present case, however, of interest is the disturbance introduced to

the flow rather than the mechanism of transition. Hence, it was decided to model the macroscopic effect of the tape rather than to fully resolve its geometry in the flow.

Several oil film surface visualization studies [20]–[22], report the formation of oil stripes downstream of ZZ tape, which are associated with streamwise vortices created by it. In other words the ZZ tape's "legs" can act as vortex generating surfaces to the incoming flow. It was hence attempted to model the trip tape in the 3D computations as a vortex generating surface using the BAY model [23]. No ZZ tape model was used in the 2D computations.

The BAY model has been found to give similar results to the fully resolved case for vortex generators on a flat plate, even though none of the two computational approaches could reproduce the experimental results fully, mainly due to excessive vorticity diffusion, see [24].

Fully resolving every leg of the trip tape in the computational model would be too expensive computationally and out of the scope of this research. Instead the ZZ tape was modelled as a limited number of attached vortex generating surfaces using the BAY model. The actual and the three simplified geometries tested are shown in Fig. 3. The "2-legged" bay model (green dashed line) was closer to the experimental results and was the one preferred for the present study.

It is important to note that the flow was always considered fully turbulent on both sides of the airfoil. That is to say that the trip tape effect was modelled macroscopically and not as a local transition point from laminar to turbulent flow. This is of course different to the experiment. However, as shown later, this approximation is good enough to qualitatively study a SC.
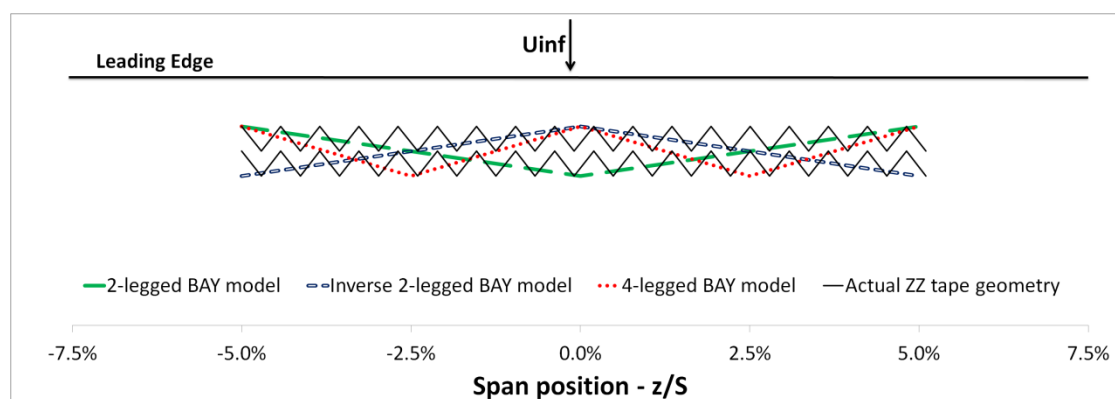

Fig. 3: Actual trip tape geometry and BAY model surfaces

Results and Discussion

In the current section both experimental and computational data (2D and 3D) are presented and discussed. First the lift (Cl) and drag (Cd) force coefficients are compared along with the relevant pressure distributions. Then a comparison of the measured and predicted SC size on the wing surface follows, along with a discussion on the wake downstream development. There is good agreement between the tests and the simulations which permits a qualitative analysis of the complex vortex structures within a SC.

Force coefficients and pressure distribution along the wing chord / span

Lift and drag curves are given in Fig. 4, Fig. 5 respectively. Data from the experiments, 3D and 2D simulations are given. For clarity, 2D data are only shown for $\alpha > 6^o$, since up to this angle there is very little difference between the 2D and the 3D computational results.

CFD predicts lift very well especially over the linear part, $\alpha < 7^o$ while the drag is overpredicted by ~0.003. The latter is connected to the fact that the simulations are fully turbulent on both sides of the airfoil and friction drag is a significant part of the Cd in attached flow conditions. At 0° XFOIL [25] predicts the pressure side free transition at 0.56c whereas the flow is laminar throughout the pressure side for angles of attack higher than 11°. The additional friction drag is partly responsible for the disagreement between the experimental and the computational value of Cd. Also, as shown in Table 1 a denser grid could have reduced the value of Cd even further. Finally, it is perhaps worth noting that estimating profile drag from the experimental pressure distributions in the wing or the wake could include significant errors, e.g. see [26].

At higher angles of attack ($\alpha > 6^o$) the 3D CFD predicted Cl follows closely the trend in the measurements with a small over-shift of 0.06. 2D CFD, however, follows a completely different trend reaching the maximum value of Cl at 12° (cf. 9° for tests and 3D simulations). This indicates that 2D simulations are not capable to describe the flow when SCs develop, as Elimelech et al. [27] also show for a much lower Re number ($O(10^4)$), though.

Over the same range of angles of attack ($\alpha > 6^o$) drag is significantly under predicted in both 2D and 3D simulations. It is noted that according to measurements at $\alpha = 7^o$ a SC is first formed on the suction side of the wing [4]. Beyond that angle the experimental Cd increases at a much higher rate due to the formation of a SC that rapidly increases in size for increasing angle of attack. In the 3D simulations, a proper SC is first formed at $\alpha = 10^o$, which leads to a local step-like decrease in Cd. This is

followed by a growing Cd at a rate similar to the tests keeping, however, the difference with respect to tests seen at ~10°.
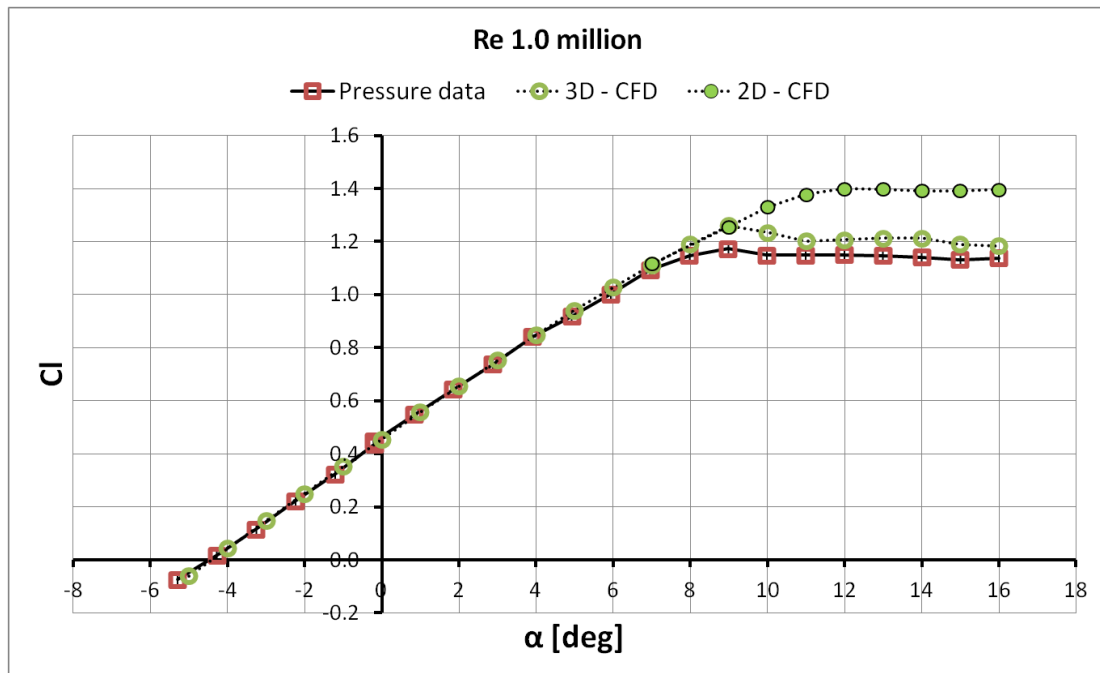

Fig. 4: Lift coefficient variation with angle of attack. Midspan value for experiments and 3D CFD. AR 2.0, Re 1.0 million.
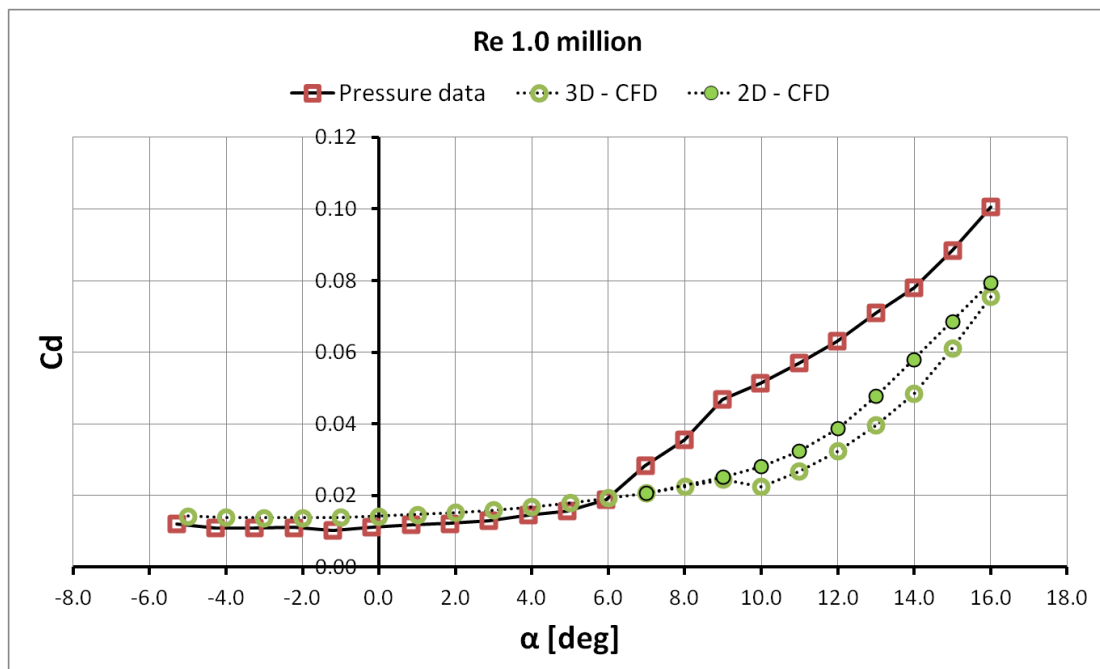

Fig. 5: Drag coefficient variation with angle of attack. Midspan value for experiments and 3D CFD. AR 2.0, Re 1.0 million.

In order to get a more detailed account on the differences between CFD simulations and measurements, the pressure coefficient distributions are compared in Fig. 6,

9

Fig. 7 and Fig. 8 for α=7°, 10° and 16°, respectively. Pressure perturbations around x=0.02% in the experimental data are due to the local effect of the ZZ tape on the pressure taps right upstream and downstream of it. The CFD pressure coefficient variation at x/c ≈ 0.4% is the result of the modelling of the ZZ tape.

At α=7° the agreement between tests and 3D CFD is still very good until the TE region is reached, see Fig. 6. A small SC is formed in the experiments but not in the computations. On the contrary there is little difference between the 2D and the 3D CFD results. At α=10° the SC is formed in the computational results, too, but it is still smaller than the one experimentally observed at the specific angle of attack, see Fig. 7. The pressure distribution prediction for the 3D case improves as the angle of attack increases, e.g. see Fig. 8 for α=16°. On the other hand the separated flow region is always significantly smaller in the 2D results.

3D CFD can provide an insight to the force variation on the wing along its span. Fig. 9 and Fig. 10 show the C_l and C_d variation along the wing span for three different angles of attack (7°, 10° and 16°). As the SC grows from its first formation (α=7°) so does the lift and drag variation with span position. Lift is always minimum at the centre of the wing span (z/S=0%) and grows towards the wing tip (z/S=50%). The drag value is also minimum at the centre of the wing span, then grows to its peak prior to the wing tip and is then reduced.

In fact, the Cp distribution at the tip (z/S=50%) is very similar to the result of the 2D computation which is also drawn in Fig. 11 for α=10°. This would suggest that the flow in that region is not affected by the SC vortex. Similar agreement was found by Elimelech et al. [27].
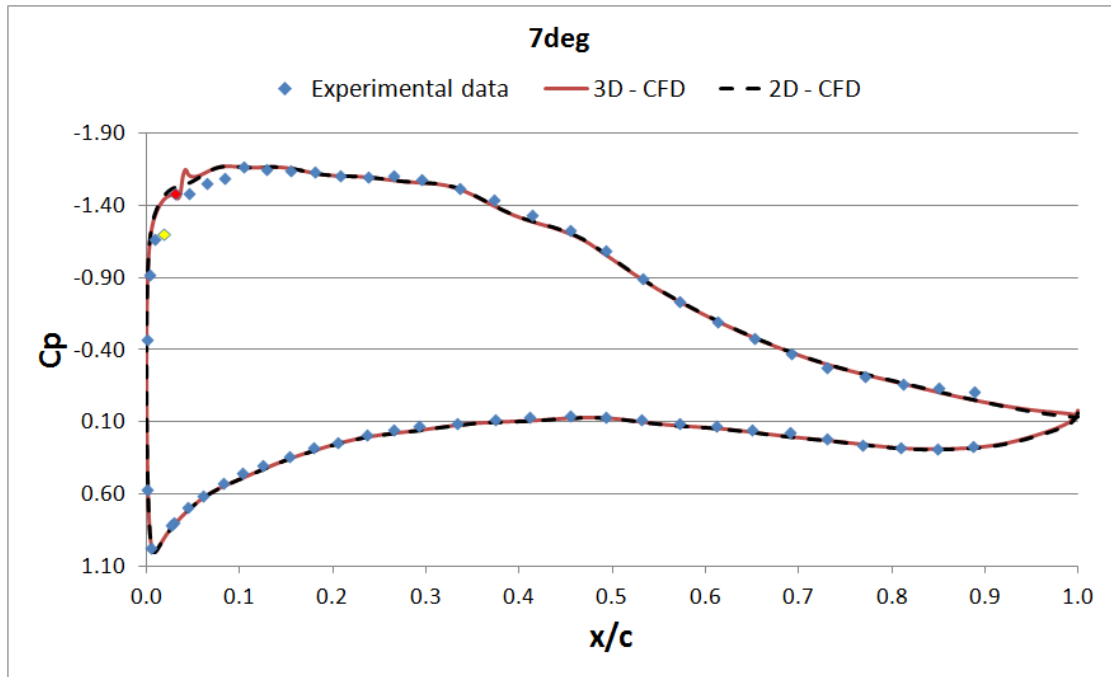
Fig. 6: Pressure coefficient distribution along the wing chord at midspan. AR 2.0, Re 1.0 million, α=7°. Yellow and red point correspond to the pressure taps just upstream and downstream of the ZZ tape, respectively,

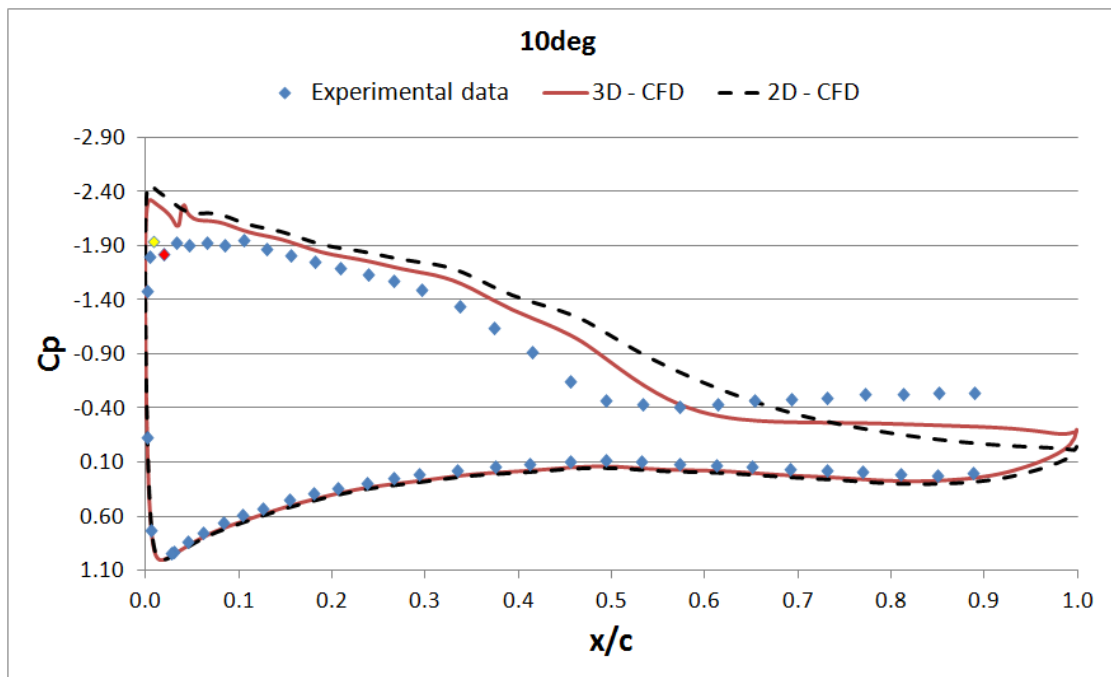Fig. 7: Pressure coefficient distribution along the wing chord at midspan. AR 2.0, Re 1.0 million, α=10°. Yellow and red point correspond to the pressure taps just upstream and downstream of the ZZ tape, respectively,
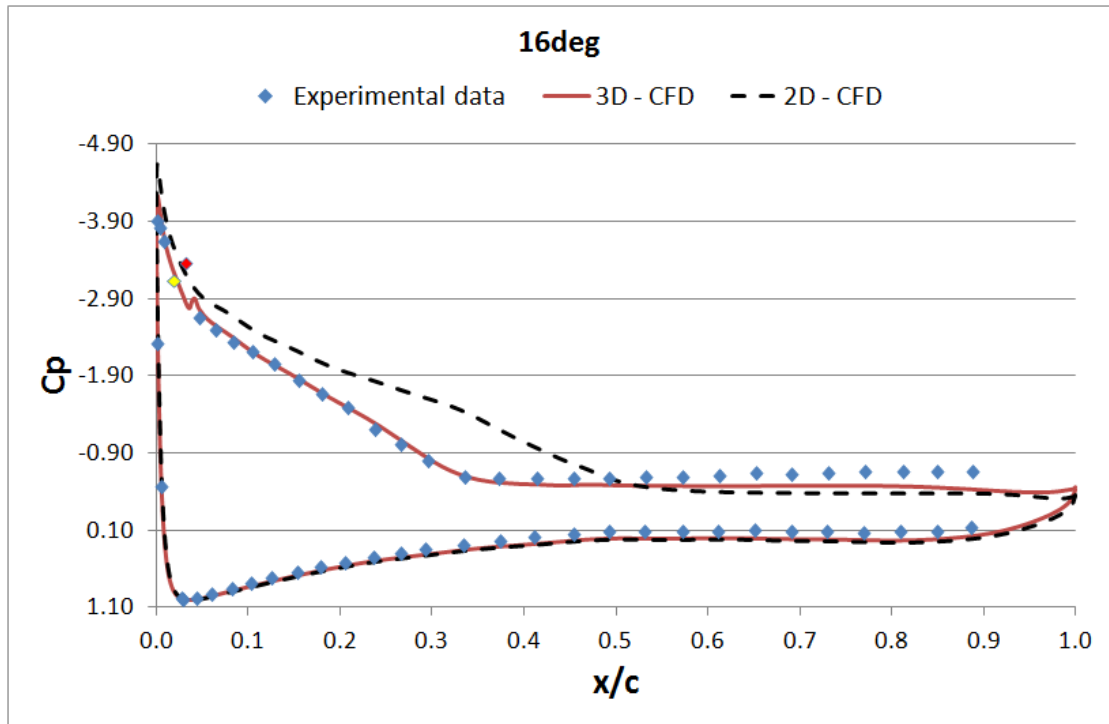
Fig. 8: Pressure coefficient distribution along the wing chord at midspan. AR 2.0, Re 1.0 million, α=16º. Yellow and red point correspond to the pressure taps just upstream and downstream of the ZZ tape, respectively.

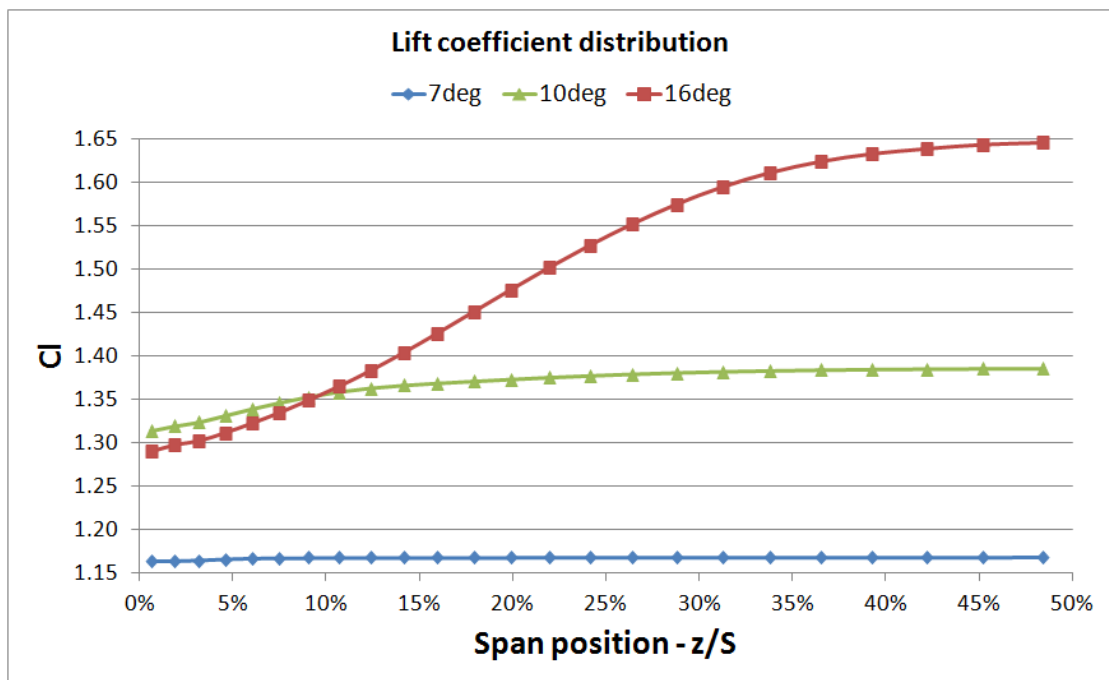**Fig. 9: Lift coefficient along the wing half span. CFD data. AR 2.0, Re 1.0 million. z/S=0% is the wing symmetry plane and z/S=50% is the wing tip.**

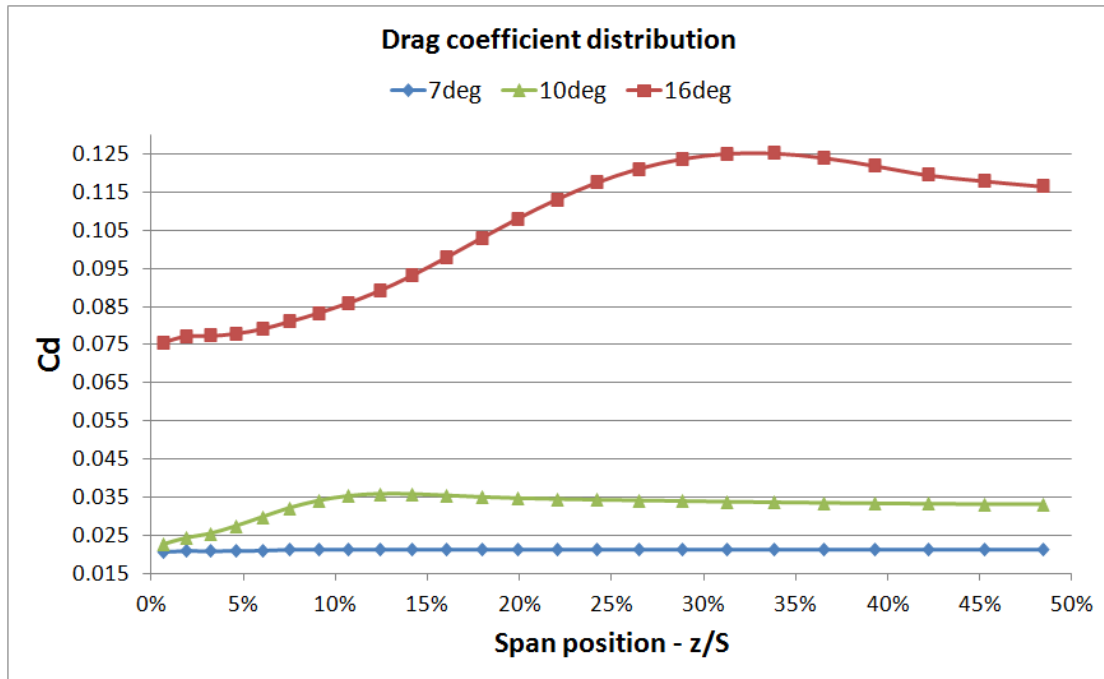Fig. 10: Drag coefficient along the wing half span. CFD data. AR 2.0, Re 1.0 million. z/S=0% is the wing symmetry plane and z/S=50% is the wing tip.
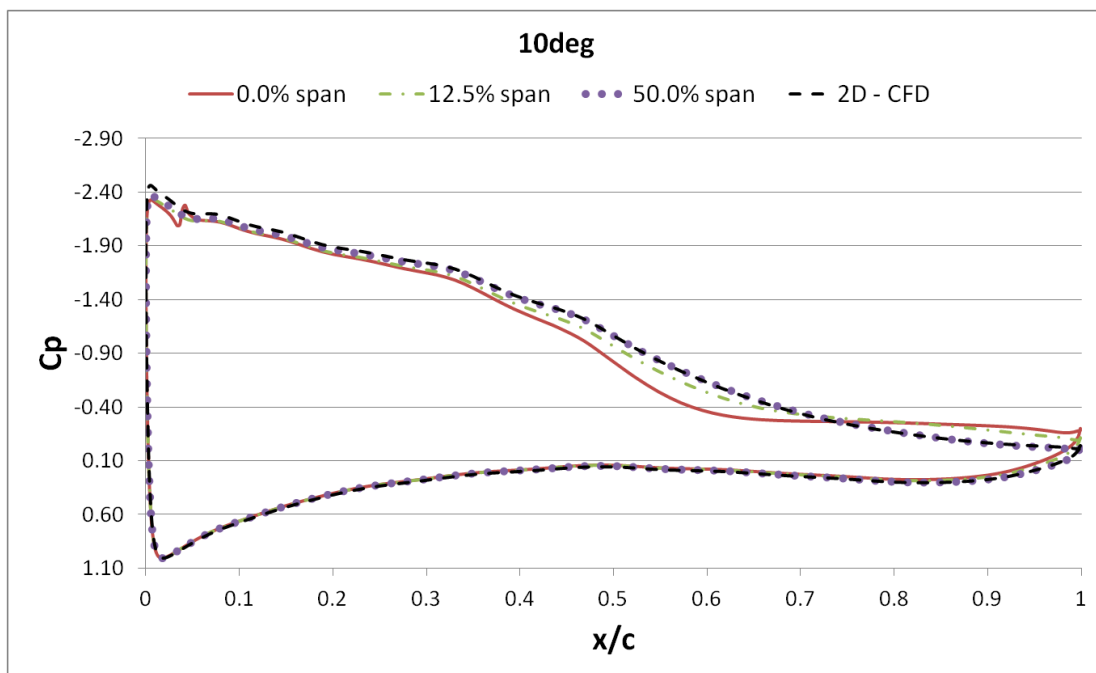

Fig. 11: Pressure coefficient distribution along the wing chord at various positions along the wing span and for the 2D solution. z/S=0% is the wing symmetry plane and z/S=50% is the wing tip. AR 2.0, Re 1.0 million.

Stall Cell size

The SC size on the wing surface is characterized by the SC maximum length (at its centre between the two vortices) and width at the TE. Fig. 12 depicts the SC chordwise length variation with respect to the angle of attack. Tuft, pressure and CFD data are compared. The agreement between the tuft and pressure data is very good. CFD correctly predicts the earliest location of separation only when α>10°.

13

Similar behaviour is observed in the SC width prediction, as Fig. 13 shows. For the CFD data the SC limit was defined as the most outboard position at which the spanwise velocity component was greater than 1% of the free stream flow.

In order to check whether this delay in predicting the SC formation is due to the modelling of the ZZ tape, CFD simulations were carried out without the ZZ tape model. In that case a SC first appears at 9 degrees, according to the tuft data from [4]. In CFD the first fully formed SC appears at 12 degrees, i.e. again with 3 degrees delay as in the case with the ZZ-tape effect switched on, see Fig. 14. This suggests that the modelling of the ZZ tape is not responsible for the delay in the SC formation which could be attributed to the turbulence model, since eddy viscosity models have known difficulties in accurately predicting 3D separation.

The exact reason for the inability of CFD to correctly predict the onset of separation remains unclear. Apart from the already mentioned unsuitability of eddy viscosity models for such a complex three-dimensional separated flow a couple of other issues could be mentioned. On one hand this was a steady state simulation of an inherently unsteady separated flow while on the other, simulations did not include the wind tunnel walls and the boundary layer on the wing fences. It is planned to investigate these aspects of the flow in the future.

It is perhaps worth noting that as in the experiments, the steady CFD simulations without the spanwise perturbation resulted in various SC combinations. In more detail, for $12^o < \alpha < 16^o$ two SCs were formed on the wing surface whereas at $\alpha = 16^o$ a combination of a single central SC along with two "half"[1] SCs at the wing tips appeared. Unlike the highly unsteady SC combinations in the tests, however, no unsteadiness was found, even when unsteady simulations were performed. It was, hence, decided to proceed with the analysis of steady simulations with the ZZ tape model switched on, as their relevance to the disturbed tests was closer.

---

[1] "Half" SC refers to only one vortex structure next to the wing tip (in this case inviscid wall) forming a "full SC" together with its mirror vortex with respect to the wall.
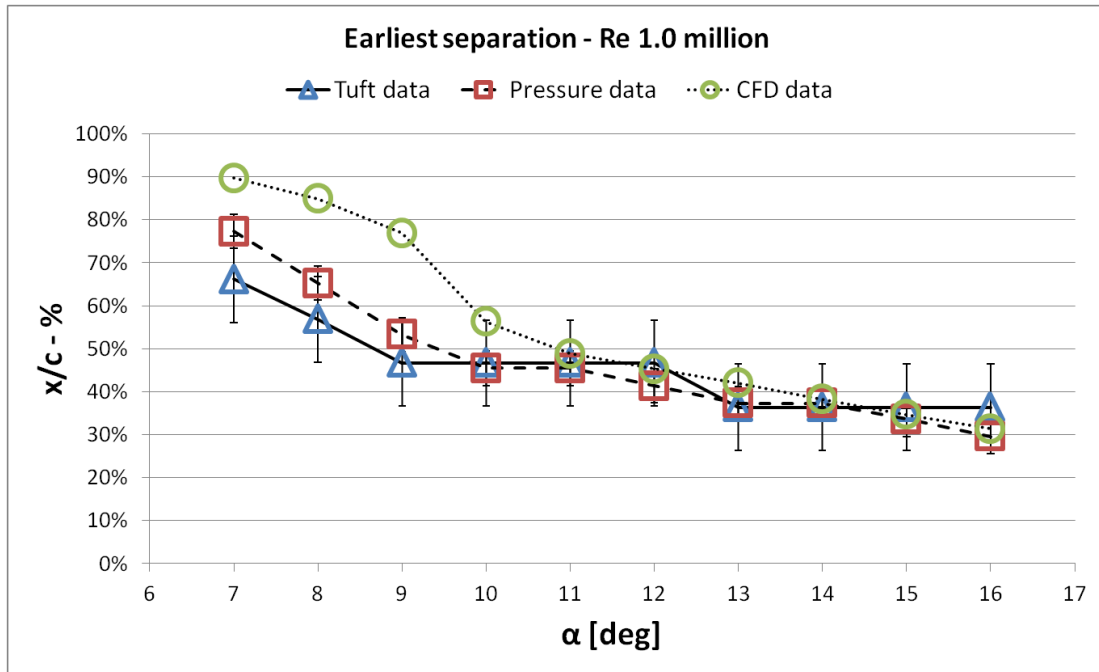
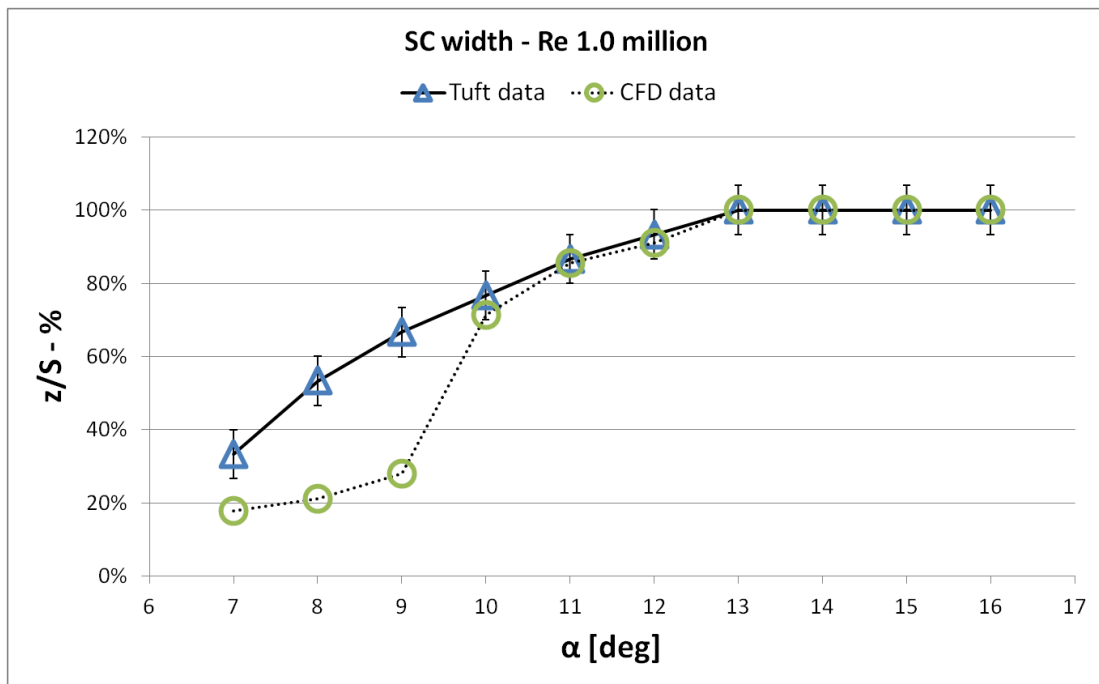**Fig. 12: Earliest separation location as found from tuft, pressure and CFD data. AR 2.0, Re 1.0 million.**

Fig. 13: SC width on the wing surface as found from tuft and CFD data, AR=2.0, Re 1.0 million.
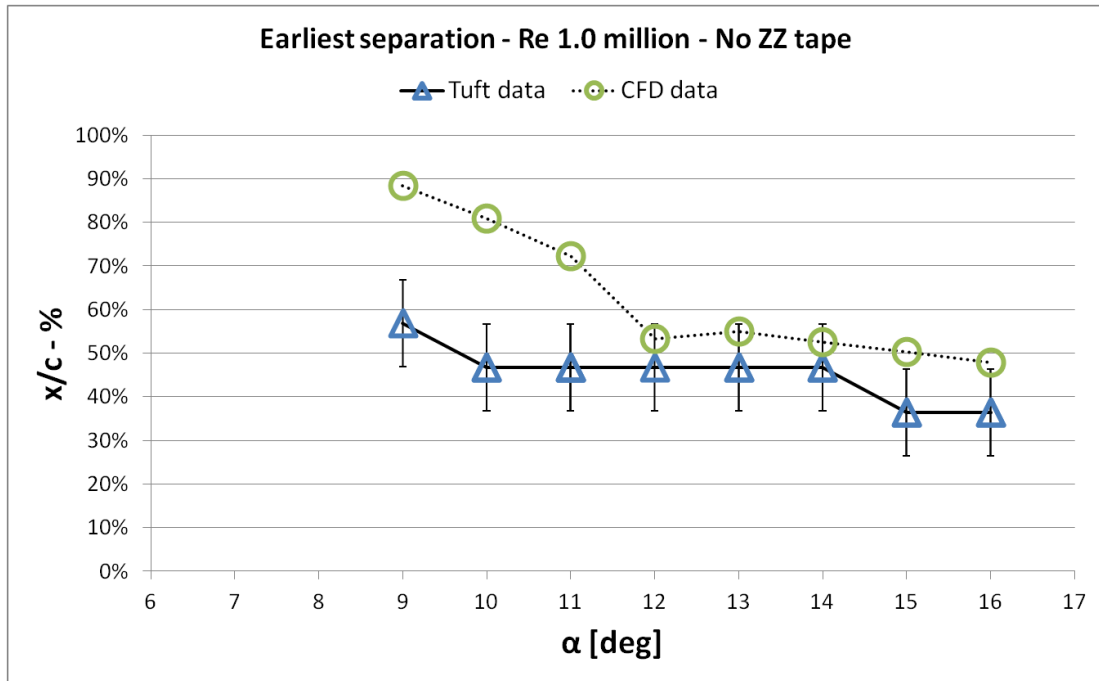
Fig. 14: Earliest separation location as found from tuft and CFD data. AR 2.0, Re 1.0 million case without ZZ tape.

Wake three-dimensionality

So far it has been made clear that the flow is highly three-dimensional on the wing surface and, unsurprisingly, so is the wake flow. A measure of the three-dimensionality of the flow is given by the wake height variation along the span. Experimentally the wake height was measured with the total pressure tubes of the wake rake (i.e. 0.8c downstream of the TE) in planes normal to the flow and the wing span. Computationally it was defined, as shown in Fig. 15, where contours of normalized total pressure on a plane normal to the flow at the rake position are shown. The area in which the SC develops in the wake is also seen in this figure. The vortex structure inside this region is discussed in a later paragraph.

In Fig. 16 the experimentally measured wake height is plotted for various angles of attack. At 0° there is small initial three-dimensionality of the flow (due to the ZZ tape) which grows substantially as the SC quickly grows after 7°. The wake shape observed by the wake pressure measurements is in qualitative agreement with Winkelmann [28] (Re number 0.48 10^6, Clark Y-14 airfoil), who studied SC wake, however, at higher angles of attack (a=21.4° and a=28.4°).

By comparing data from Fig. 13 and Fig. 16 it is possible to examine the SC evolution in the wake. For example at 10° the SC width at the wing suction surface is approximately 76% of the wing span (Fig. 13) whereas the SC extends approximately from -20% to 20% of the span 0.8c downstream of the TE. This suggests that the SC contracts in the spanwise direction as it moves downstream and a similar behaviour is observed throughout the angle of attack range. As shown next, this is due to the vortex interaction inside the SC above the wing surface.

16

In general CFD predicts well the (parabolic) shape of the SC wake but underpredicts the wake size, e.g. see Fig. 17 and Fig. 18 where the relevant CFD and experimental data are compared for 10 and 16 degrees, respectively. Even though CFD offers a good prediction for SC size on the wing surface at 16° (see Fig. 12 and Fig. 13) it fails to do so further downstream (Fig. 18). This could possibly be attributed to excessive vorticity diffusion inside the wake. Still the general shape of the wake appears correct and permits a qualitative analysis.

The distance between the wake rake total pressure tubes ranged from 6mm at its centre to 15mm at its sides. The maximum uncertainty for the wake height measurement was then +/- 30mm or 0.05c, which is the value indicated by the error bars in Fig. 17 and Fig. 18.
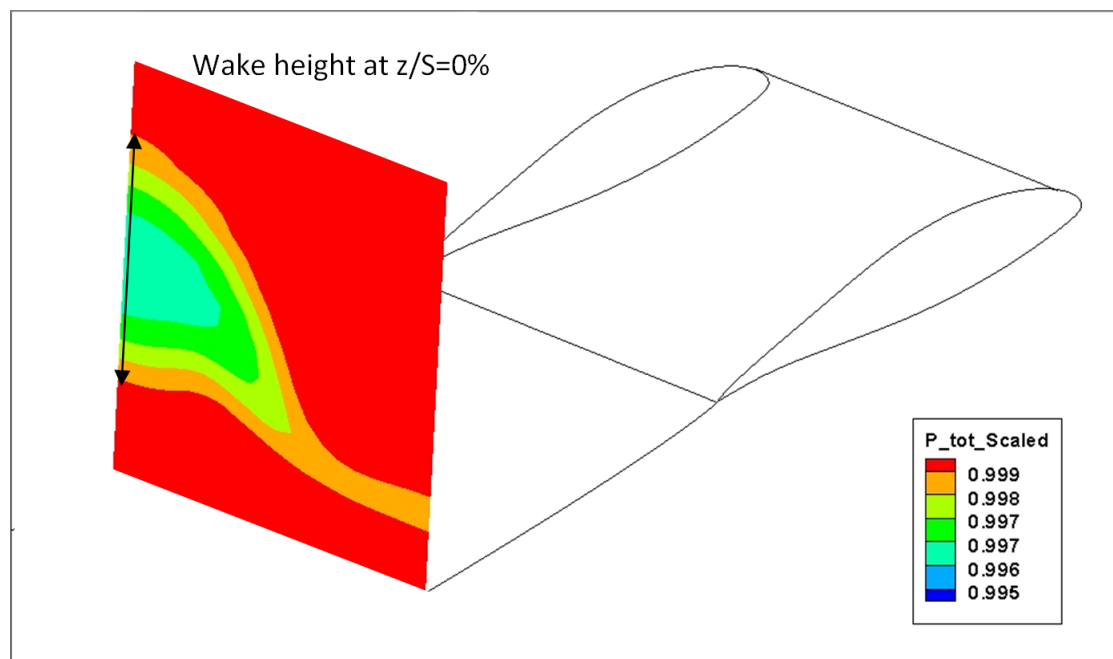

Fig. 15: Contours of normalized total pressure on a plane normal to the free stream at the rake position (0.8c downstream of the TE). The definition of the wake height is also shown for z/S=0% span. Symmetry plane is at the left of the picture.
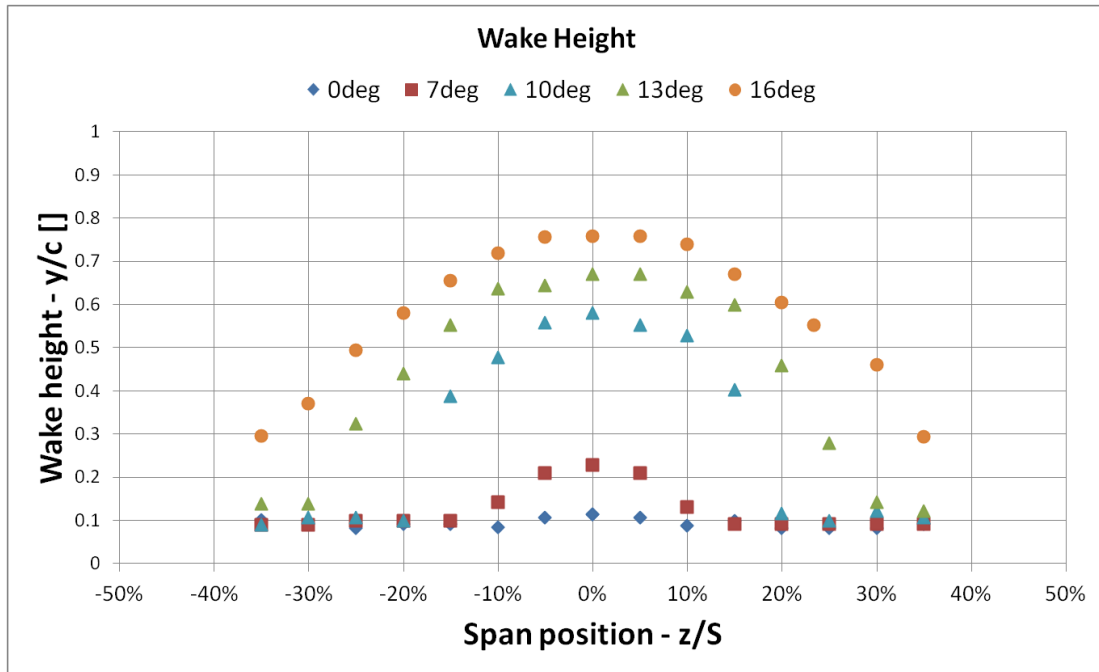
Fig. 16: Wake height at the rake position (0.8c downstream of the TE) for AR=2.0, Re=1.0x10^6 and α=0°, 7°, 10°, 13° and 16°. Error bars not included for clarity.

Fig. 17: Wake height at the rake position (0.8c downstream of the TE) for α=10 degrees based on experimental and CFD data. CFD data were only available for half span due to the symmetry condition and where are mirrored for the other half of this graph. 2nd order trendlines are drawn over the data from -15% to 15% span. Error bars value is 0.05c.
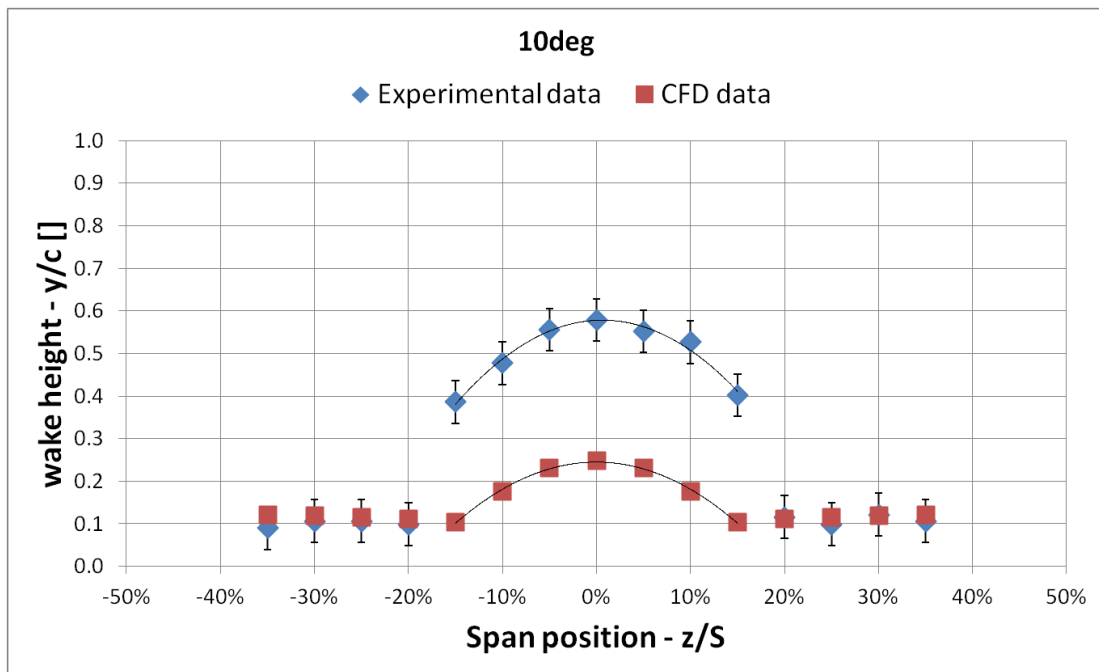
Fig. 18: Wake height at the rake position (0.8c downstream of the TE) for α=16 degrees based on experimental and CFD data. CFD data were only available for half span due to the symmetry condition and where are mirrored for the other half of this graph. 2nd order trendlines are drawn over the data from -35% to 35% span. Error bars value is 0.05c.
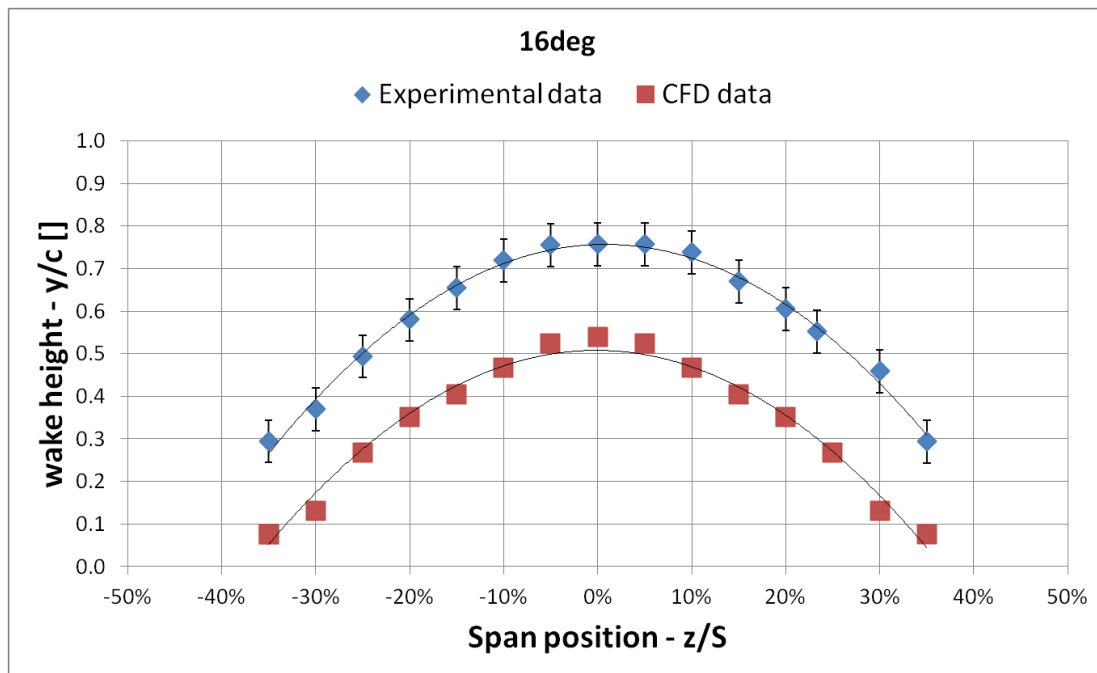
Vortex structures

In an early study Winkelmann and Barlow [18] proposed a "tentative flow model" in an attempt to explain the SC structure. It was then suggested that the two nodes observed on the wing surface are "the time averaged effect of a vortex flow that loops from one node to the other". However, in a later article, Yon and Katz [7] showed that this model was inconsistent with their pressure data and argued that if the SC vortices trailed downstream the induced flowfield would be in agreement with their measurements.

In this section an attempt is made to gain insight into the structure of SCs based on the CFD results. As discussed next, the CFD data suggest that SC vortices start from the wing surface and continue downstream in the wake as suggested in [7]. At the same time the SC vortices interact with the *separated line vortex* and the *TE line vortex* (definitions of the basic line vortices are given in the following paragraphs).

The discussion focuses on the case of 16° angle of attack at which the overall CFD flow characteristics match best with the measured data. Surface stream lines, in-plane stream lines on x- and z-planes in combination with contours and iso surfaces of the Q criterion [29] are used for the analysis. In-plane stream lines are, of course, artificial, unless the flow has zero velocity normal to the plane under consideration. However, they can provide indication on vortex location and improve the understanding of the flow.

Fig. 19 shows surface stream lines on the wing surface and in-plane stream lines on several z- planes. The SC vortex can be clearly seen on the wing surface (with vortex centre at z/S≈37%) while on the z planes, two spanwise line vortices of opposite vorticity can be detected. The one here named "*separated line vortex*" (SLV) stands above the wing surface while the other named "*TE line vortex*" (TELV) is aligned with the TE and is located in a short downstream distance of it. Both have cores that increase in size when moving from tip to the centre of the SC. The increase of the core size is bigger for the SLV which undergoes substantial upstream deflection when approaching the mid-span. On the contrary the deflection of the TELV is smaller and for most of its length remains almost parallel to the TE.

In order to examine how the SLV and the TELV develop in space a more detailed look at the in-plane flow lines of Fig. 19 is needed. Fig. 20 is a side view of Fig. 19, but now flow lines are limited to the vortex core regions. In-plane flow lines are coloured by their spanwise position, which is indicated on the figure. It is clear that the SLV core moves upwards and upstream towards the centre of the SC (z/S = 0%). Note that the flow lines corresponding to the TELV core do not form circles towards the side of the SC (z/S=50%) where the vortex is weaker, but they do so at the centre of the SC. The TELV core appears to move upwards and downstream towards the centre of the SC (z/S=0%). A possible explanation for the vortex cores movement could be that the SC vortex pushes the separation line as well as the inboard part of the SL vortex, upstream over the midspan plane. Thus the SL vortex grows and as a result the TE line vortex grows and is pushed downstream.
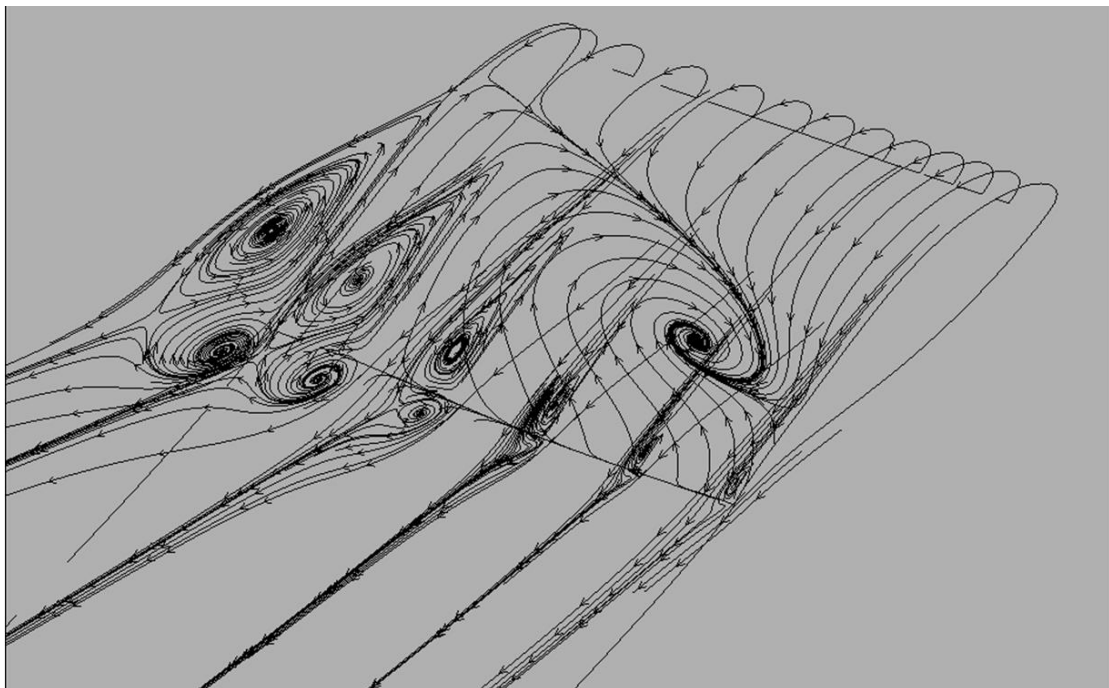

Fig. 19: Surface flow lines on the wing suction surface along with in-plane flow lines on planes z/S=0% (symmetry plane), z/S=10%, z/S=20%, z/S=30%, z/S=40%, z/S=50% (wing tip, right hand side). Wing half span only. AR 2.0, Re 1.0 million, α=16 degrees.
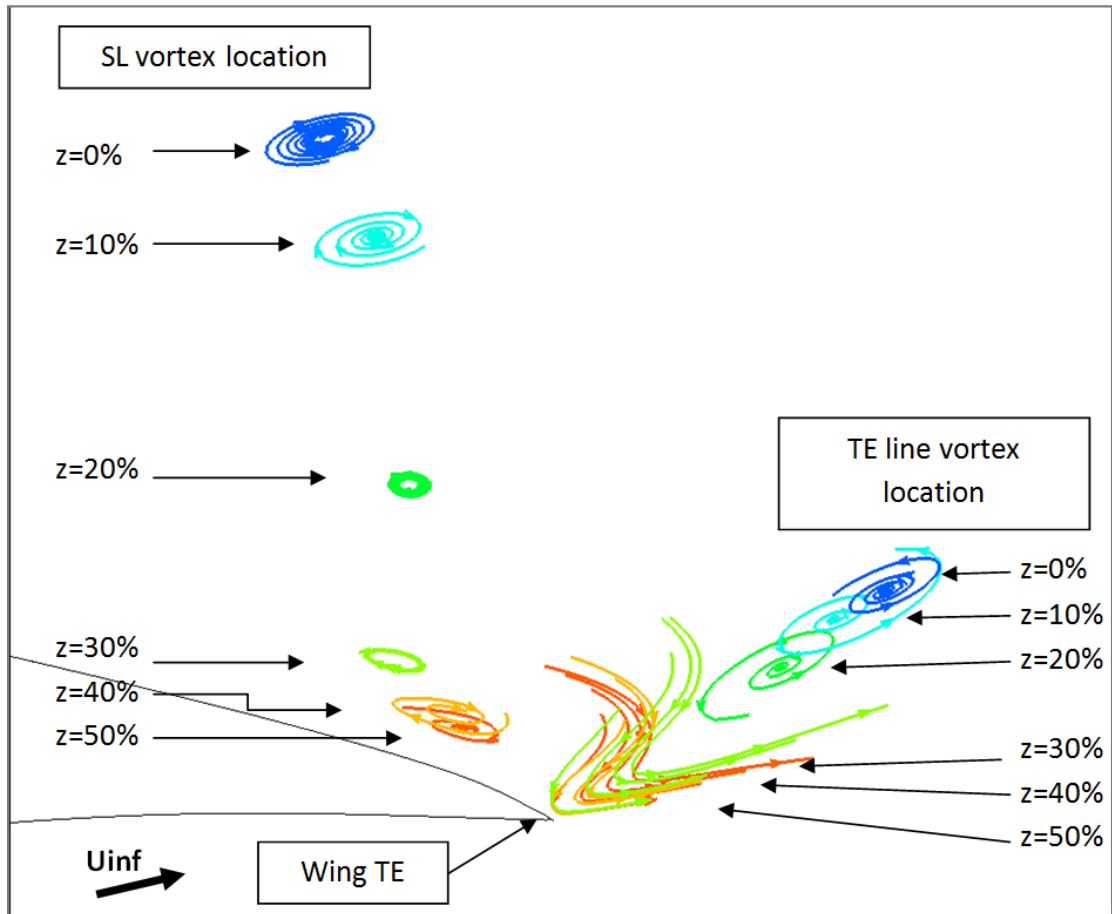
Fig. 20: Side view detail of the wing TE. In-plane flow lines coloured by z dimension on planes at z/S=0% (symmetry plane), z/S=10%, z/S=20%, z/S=30%, z/S=40%, z/S=50% (tip). AR 2.0, Re 1.0 million, α=16 degrees.

At the same time, the SLV affects the development of the SC vortex. Fig. 21 shows flow lines on the wing suction surface and in-plane stream lines on two planes normal to wing span (z/S=30%, z/S=10%) and one normal to the free stream flow (at the TE, x=1). It is observed that by the time the SC vortex has reached the TE it has already moved inboard compared to its node on the wing suction surface. It is conceivable that this happens because from tip to mid span, the core of the SLV grows, its centre moves in the positive z direction and the negative x direction (see Fig. 20), and therefore attracts the SC vortex inboard.

Fig. 22 shows in-plane stream lines and Q contours on planes vertical to the flow at x=1.0 (TE), x=2.0 and x=3.0. In the planes at x=2.0 and x=3.0 the Q contour gives a clearer indication of the SC vortex location. This is not the case for the plane at x=1.0 because at that location multiple vortices are present, as already discussed. Looking at the in-plane stream lines, however, the vortex core can be located at about z/S=17.5% for all the downstream planes. This suggests that after the initial inboard shift of the SC vortex, no significant spanwise movement occurs in the wake.
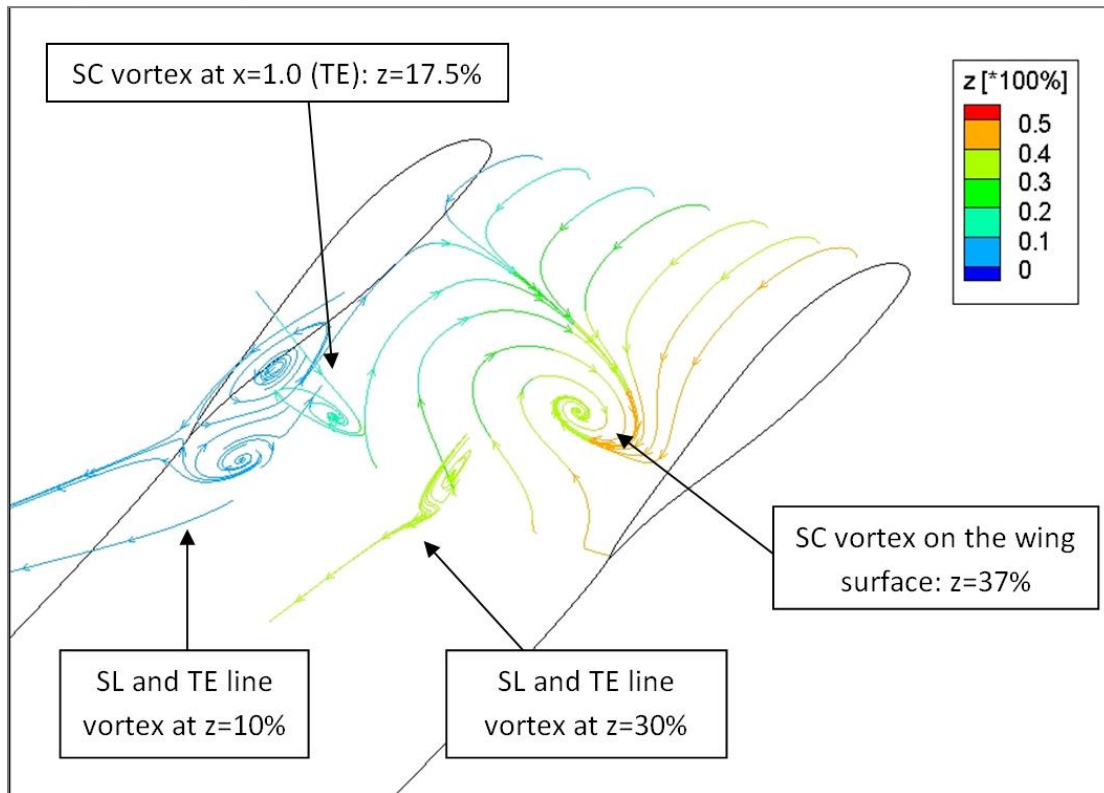
Fig. 21: Surface flow lines on the wing suction surface. in-plane flow lines on planes z/S=10% and z/S=30% (normal to the wing span) and x=1.0 (normal to the free stream at the TE). All flow lines are coloured by spanwise location. Symmetry plane is at the left hand side (z/S=0%). AR 2.0, Re 1.0 million, α=16 degrees.
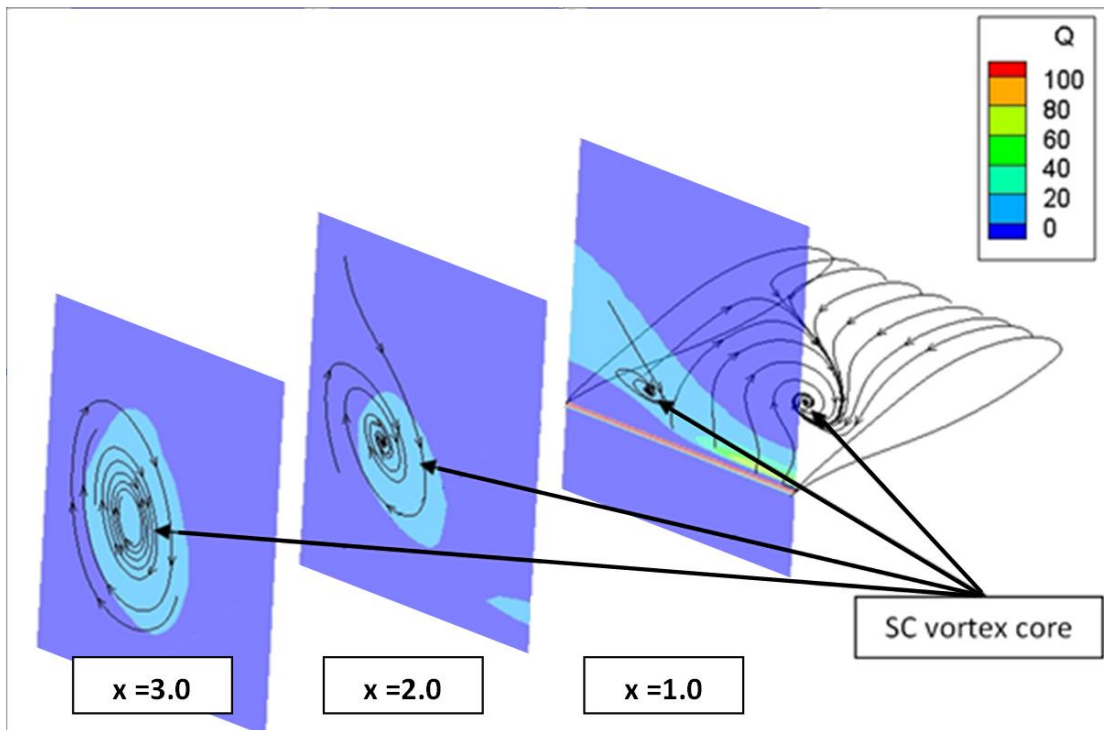

Fig. 22: Surface flow lines on the wing suction surface along with in-plane flow lines and Q contours on planes normal to the free stream flow at x=1.0 (TE), x=2.0 and x=3.0. Vortex core spanwise location is z/S=37% on the wing surface and z≈17.5% in the downstream planes. Symmetry plane is at the left hand side (z/S=0%). AR 2.0, Re 1.0 million, α=16 degrees.

A qualitative visualization of the vortex core lines based on Q isosurface locations is given in Fig. 23 along with the vorticity direction. One can distinguish three continuous surfaces.

  a. One corresponding to the TELV
  b. One that includes the SLV and the initial part of the SC vortex.
  c. One that stands for the continuation of the SC vortex in the wake.

The gap along the SC core line could possibly be attributed to the inadequacy of the Q criterion when a vortex expands in a non-uniform strain field [30].

It is possible that the SC vortex starts normal to the wing suction surface, but is quickly deflected by the SL vortex and the oncoming flow. By the time the SC vortex reaches the wing TE, it has moved inboard and its vorticity is parallel to the free stream flow.
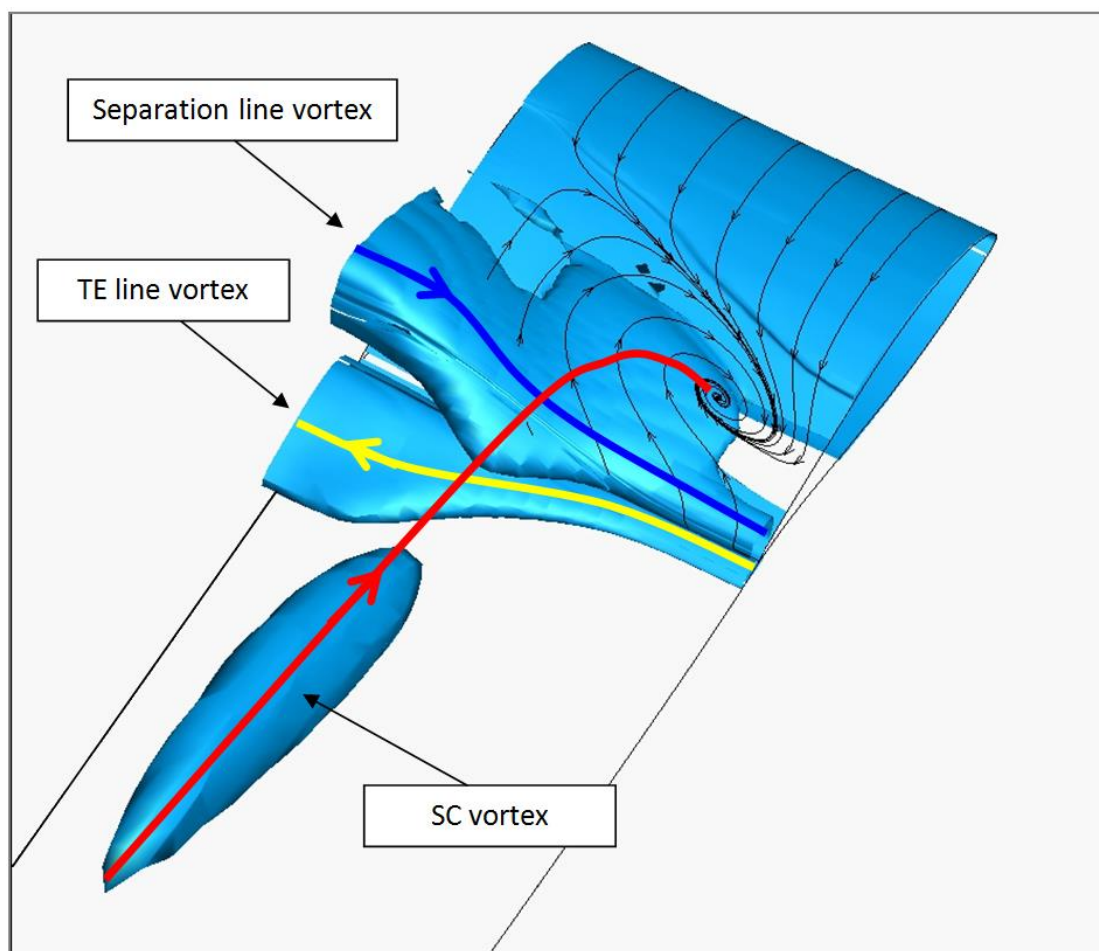

Fig. 23: Surface flow lines on the wing suction surface and Q isosurface for Q=1. Interpreted vortex core lines with vorticity direction also shown. Symmetry plane is at the left hand side (z/S=0%). AR 2.0, Re 1.0 million, α=16 degrees.

Finally Fig. 24 shows surface flow lines on the wing suction surface along with in plane flow lines and velocity magnitude contours on planes normal to the free stream flow at x=1.0 (TE), x=2.0 and x=3.0. As the SC vortex moves downstream it interacts with its symmetric vortex pushing each other higher and at the same time deforming the wing wake, pushing it lower at the tips and higher at the centre of the SC.
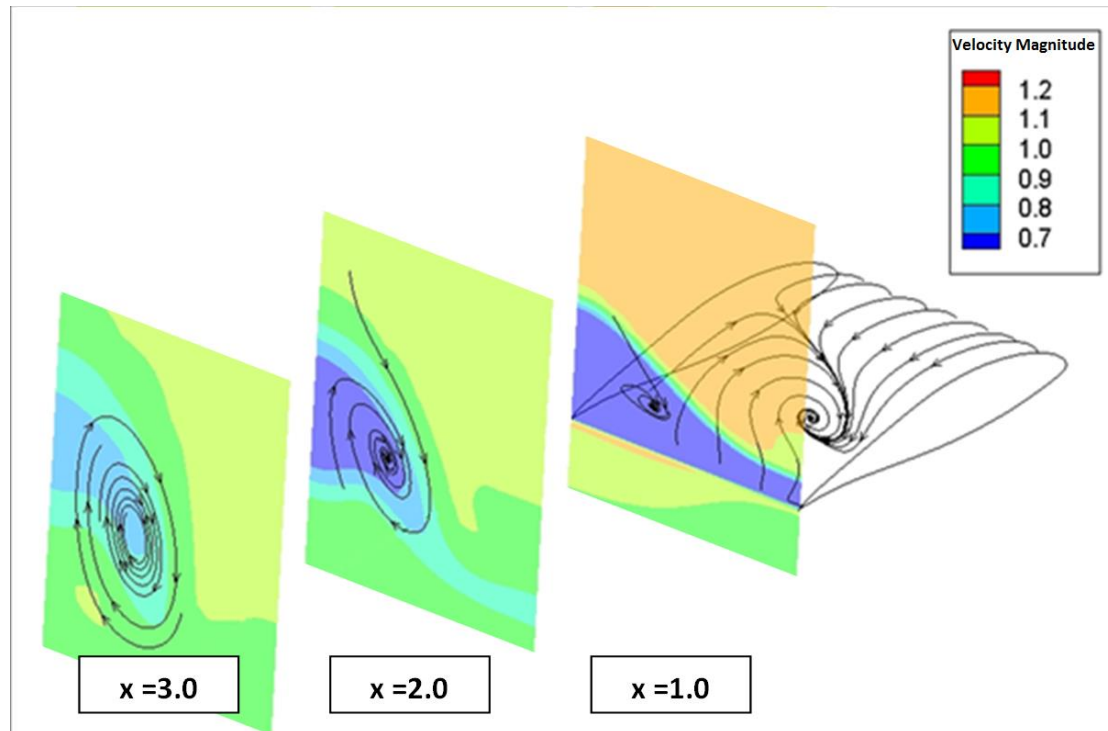

Fig. 24: Surface flow lines on the wing suction surface along with in-plane flow lines and velocity magnitude contours on planes normal to the free stream flow at x=1.0 (TE), x=2.0 and x=3.0. Symmetry plane is at the left hand side (z/S=0%). AR 2.0, Re 1.0 million, α=16 degrees.

Conclusions

The flow over a rectangular wing was studied both experimentally and computationally. At higher angles of attack inherently unstable SCs were formed on the suction side of the wing. The flow was stabilized by using a ZZ tape strip locally as a spanwise disturbance, see [4]. In the 3D simulations the macroscopic effect of ZZ tape was modelled as a pair of vortex generating surfaces using the BAY model.

Using the experimental and CFD data in comparison, the following conclusions can be drawn:

1. There is good qualitative and quantitative agreement between experimental and CFD data until a SC is first formed (α<7º).
2. At higher angles, α>7º, the 3D CFD data reproduce the experimental data with a 3º delay which allows a trustworthy qualitative analysis of the vortex structures inside a SC.

3. The SC vortices start normal to the wing surface and extend downstream in the wake in agreement with the model suggested by Yon and Katz [7].
4. The SC vortices interact strongly with the SL and the TEL vortices:
    a) By the time the SC vortex line reaches the wing TE it has already been deflected inboard and aligned with the free stream flow.
    b) The SL and TEL vortex cores grow and move higher towards the SC centre.
5. Due to the inboard deflection of the SC vortices the SC trace in the wake contracted in the spanwise direction compared to the SC width on the wing surface.
6. The three-dimensionality of the flow results in a significant spanwise variation of the force coefficients. In all cases sectional Lift and drag attain their minimum value at the centre of the SC.
7. Well away from the SC vortex, the pressure distribution becomes similar to that of a 2D flow.
8. Under the influence of the SC vortices the wing wake is pushed upwards at the centre of the SC and downwards at the sides.

Acknowledgements

References

[1] A. Winkelmann, "An experimental study of mushroom shaped stall cells," AIAA PAPER 82 - 0942, 1982.

[2] C. Velte, M. Hansen, K. Meyer, and P. Fuglsang, "SPIV study of passive flow control on a WT airfoil," presented at the EWEA Torque, Heraklion, 2010.

[3] P. Fuglsang and S. Bove, "Wind Tunnel Testing Of Airfoils Involves More Than Just Wall Corrections," presented at the European Wind Energy Conference, Brussels., 2008.

[4] M. Manolesos and S. Voutsinas, "Geometrical characterization of stall cells on rectangular wings," *Wind Energy*, submitted for publication 06/2012.

[5] N. Gregory, V. Quincey, C. O'Reilly, and D. Hall, "Progress Report on Observations of Three-Dimensional Flow Patterns obtained during Stall Development on Aerofoils, and on the Problem of Measuring Two-Dimensional Characteristics," British A.R.C.C.P. 1146, 1971.

[6] N. Sorensen and S. Schreck, "Computation of the NREL Phase-VI Rotor In Pitch Motion During Standstill," presented at the EWEA Torque, Herakleion, 2010.

[7] S. Yon and J. Katz, "Study of the Unsteady Flow Features on a Stalled Wing," *AIAA Journal*, vol. 36, no. 3, pp. 305–312, 1998.

[8]   N. Gregory and C. L. O'Reilly, "Low-speed aerodynamic characteristics of NACA 0012 aerofoil section, including the effects of upper-surface roughness simulating hoar frost," 3726, 1970.

[9]   T. Zarutskaya and R. Arieli, "On Vortical Flow Structures at Wing Stall and Beyond," in *35th AIAA Fluid Dynamics Conference and Exhibit*, Toronto, 2005, pp. 1–10.

[10] A. P. Broeren and M. B. Bragg, "Spanwise Variation in the Unsteady Stalling Flowfields of Two-Dimensional Airfoil Models," *AIAA Journal*, vol. 39, no. 9, pp. 1451–1461, 2001.

[11] D. Rodríguez and V. Theofilis, "On the birth of stall cells on airfoils," *Theoretical and Computational Fluid Dynamics*, vol. 25, no. 1–4, pp. 105–117, Mar. 2010.doi: 10.1007/s00162-010-0193-7

[12] D. Mourikis, V. Riziotis, and S. Voutsinas, "Optimum aerodynamic design of 52m blade for a prototype 5MW WEC." NTUA Technical Report, 2005.

[13] J. B. Barlow, W. H. Rae, and A. Pope, *Low-Speed Wind Tunnel Testing*, 3rd ed. Wiley-Interscience, 1999.

[14] M. Manolesos and S. Voutsinas, "3D flow separation on plane wing." [Online]. Available: http://www.aerolab.mech.ntua.gr/3D_flow_separation_on_plane_wing_1.html . [Accessed: 27-Jul-2011].

[15] P. R. Spalart and S. R. Allmaras, "A one-equation turbulence model for aerodynamic flows," presented at the 30th Aerospace Sciences Meeting and Exhibit, NV, US, 1992.

[16] F. R. Menter, "Zonal two-equation k-w turbulence model for aerodynamic flows," *AIAA Paper*, vol. 1993–2906, 1993.

[17] R. Rubinstein, C. L. Rumsey, M. D. Salas, and J. L. Thomas, "Turbulence Modeling Workshop," ICASE Interim Report 37, 2001.

[18] A. Winkelmann and J. Barlow, "Flowfield Model for a Rectangular Planform Wing beyond Stall," *AIAA*, vol. 18, no. 08, pp. 1006–1008, 1980.

[19] G. E. Elsinga and J. Westerweel, "Tomographic-PIV measurement of the flow around a zigzag boundary layer trip," *Experiments in Fluids*, no. 1957, pp. 05–08, 2011. doi: 10.1007/s00348-011-1153-8

[20] C. A. Lyon, M. S. Selig, and A. P. Broeren, "Boundary Layer Trips on Airfoils at Low Reynolds Numbers," presented at the AIAA 35th Aerospace Sciences Meeting, Reno, NV, 1997, vol. 97–0511.

[21] L. M. M. Boermans, "Research on sailplane aerodynamics at Delft University of Technology. Recent and present developments.," *Netherlands Association of Aeronautical Engineers NVvL*, Jan. 1997.

[22] G. M. R. Van Raemdonck and M. J. L. Van Tooren, "Time averaged phenomenological investigation of a wake behind a bluff body," presented at the BBAA VI International Colloquium on: Bluff Bodies Aerodynamics & Applications, Milano, Italy,, 2008.

[23] E. E. Bender, B. H. Anderson, and P. J. Yagle, "Vortex generator modeling for Navier-Stokes codes," *ASME Paper FEDSM99-6919*, 1999.

[24] J. Dudek, "Modeling Vortex Generators in the Wind-US Code," Technical Memorandum NASA/TM-2010-216744, Jul. 2010.

[25] M. Drela, "XFOIL: An Analysis and Design System for Low Reynolds Number Airfoils," in *Low Reynolds Number Aerodynamics*, vol. 54, T. J. Mueller, Ed. NY, US: Springer-Verlag, 1989, pp. 1–12.

[26] H. J. Goett, *Experimental Investigation of the Momentum Method for Determining Profile Drag*. National Advisory Committee for Aeronautics, 1939.

[27] Y. Elimelech, R. Arieli, and G. Iosilevskii, "The three-dimensional transition stages over the NACA-0009 airfoil at Reynolds numbers of several ten thousand," *Physics of Fluids*, vol. 24, no. 2, p. 024104, 2012.doi: 10.1063/1.3682377

[28] A. Winkelmann, "An experimental study of separated flow on a finite wing," AIAA PAPER 81-1882, 1981.

[29] J. C. R. Hunt, A. A. Wray, and P. Moin, "Eddies, streams, and convergence zones in turbulent flows," Center for Turbulence Research Report CTR-S88, 1988.

[30] J. Jeong and F. Hussain, "On the identification of a vortex," *Journal of Fluid Mechanics*, vol. 285, no. -1, pp. 69–94, 1995. doi: 10.1017/S0022112095000462

Case	Far field boundary distance	Domain Size	Earliest Separation Point	Cl at midspan	Cd at midspan
20c	20c	(250x110x24) 0.66 10^6 cells	75.9%	1.31762	0.02858
50c (Baseline)	50c	(280x140x24) 0.94 10^6 cells	76.9%	1.32475	0.02461
Increased spanwise density	50c	(250x110x40) 1.10 10^6 cells	75.5%	1.33550	0.02379
Increased density in x and y directions.	50c	(470x230x24) 2.59 10^6 cells	79.4%	1.33915	0.02290

Table 1: Computational details and selection of results for the different computational grids tested. a=9.0deg, Re=10^6.